

## Neutron scattering investigation of the spin-flop transition in $\text{MnCl}_2 \cdot 4\text{D}_2\text{O}$

R. A. Butera

*Department of Chemistry, University of Pittsburgh, Pittsburgh, Pennsylvania*

L. M. Corliss, J. M. Hastings, and R. Thomas

*Department of Chemistry, Brookhaven National Laboratory, Upton, New York 11973*

D. Mukamel

*Department of Nuclear Physics, The Weizmann Institute of Science, Rehovot, Israel  
and I.B.M. T. J. Watson Research Center, Yorktown Heights, New York 10566*

(Received 10 March 1981)

A detailed study of the spin-flop transition in  $\text{MnCl}_2 \cdot 4\text{D}_2\text{O}$  has been carried out. The characteristics of the first-order "shelf," as determined by neutron scattering, were found to be in good agreement with the phase diagram derived here for the appropriate monoclinic symmetry. Experimental and theoretical analysis of the critical scattering observed at the spin-flop transition close to the bicritical point provide independent confirmation of the first-order nature of the transition.

### I. INTRODUCTION

Anisotropic antiferromagnetic materials exhibiting bicritical points have been the subject of considerable theoretical and experimental investigation.<sup>1-29</sup> These efforts have sought to determine the nature and extent of the magnetic phase transition boundaries in  $(\vec{H}, T)$  space. The case of uniaxial anisotropy has been treated theoretically by Rohrer and Thomas<sup>3</sup> using a mean-field approach and then by Fisher *et al.*<sup>2</sup> using renormalization-group calculations. In the orthorhombic case the predicted phase diagram<sup>7</sup> is shown schematically in Fig. 1 where  $H_{\parallel}$ ,  $H_{\perp m}$ , and  $H_{\perp h}$  are the fields applied parallel to the easy, the medium, and the hard anisotropy axes, respectively. The system exhibits paramagnetic (PM) behavior for all field and temperature values which are outside the critical surfaces. Within these surfaces the system exists in an antiferromagnetic (AF) phase at low fields and in a spin-flopped (SF) phase at high fields. The AF-SF transition boundary is first order and is shown as a shaded region in Fig. 1. When the field is tilted in the  $(H_{\parallel}, H_{\perp m})$  plane, but is kept perpendicular to the  $H_{\perp h}$  direction, the AF-SF transition boundary exists only over a small range of tilt angles and does not contact the critical surface. However, when the field is tilted in the  $(H_{\parallel}, H_{\perp h})$  plane and kept perpendicular to the  $H_{\perp m}$  direction, the AF-SF transition boundary extends to the critical surface, where it terminates in a bicritical line. For the case of orthorhombic anisotropy, these predictions have been confirmed experimentally over a range of tilt angles in  $\text{GdAlO}_3$ , by Rohrer and coworkers.<sup>6-9</sup> Symmetry analysis of  $\text{MnCl}_2 \cdot 4\text{D}_2\text{O}$  (see Sec. II) indicates that

the phase diagram of this monoclinic compound should also be qualitatively given by Fig. 1. This analysis also indicates that the two critical surfaces (AF-PM and SF-PM) are associated with  $n = 1$  component order parameters, while the bicritical line corresponds to an  $n = 2$  component order parameter.

Manganese chloride tetrahydrate has been studied extensively.<sup>10-29</sup> Zalkin *et al.*<sup>14</sup> determined the crystal structure and heavy atom positional parameters by x-ray diffraction. El Saffar and Brown<sup>23</sup> obtained a refinement of the hydrogen positions by neutron diffraction. The magnetic structure was investigated by Spence and Nagarajan<sup>15</sup> using NMR techniques and by Altman *et al.*<sup>25</sup> using neutron diffraction. Altman *et al.* concluded that the spins were collinear and that the projection of the spin on the  $ac$  plane was  $2.8^\circ \pm 1.4^\circ$  from the  $c^*$  axis toward the  $c$  axis and the projection of the spin on the  $bc^*$  plane was  $0.5^\circ \pm 0.5^\circ$  from  $c^*$  towards  $b$ , where the asterisk denotes a reciprocal axis. The crystallographic and anisotropy axes deduced from these studies are shown in Fig. 2. Anticipating results to be presented later, the easy axis in the figure is taken to lie in the  $ac$  plane. Rives and coworkers<sup>16,24,26</sup> investigated the phase diagram using differential magnetic susceptibility measurements with the applied field directed along the  $c^*$ ,  $b$ , and  $a$  axes, as well as  $2.8^\circ$  from the  $c^*$  axis toward the  $c$  axis. For the latter alignment as well as for the  $c^*$  direction, their results indicated first-order behavior for the AF-SF transition only for temperatures less than 0.37 K, whereas the bicritical point is reported to occur at 1.22 K. Giaouque and coworkers<sup>17-20</sup> investigated the phase diagram using heat capacity, magnetization, and the adiabatic variation of

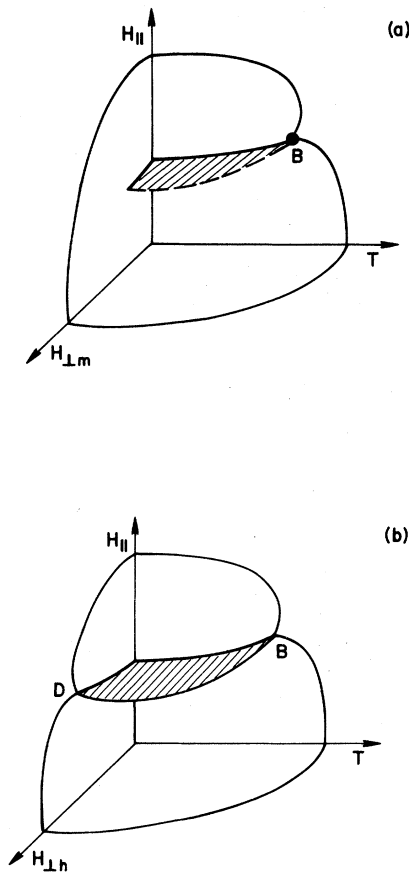


FIG. 1. The phase diagram of uniaxial antiferromagnets exhibiting a bicritical point.  $H_{\parallel}$ ,  $H_{\perp m}$ , and  $H_{\perp h}$  are the components of the magnetic field in the easy, medium, and hard directions, respectively. (a) The  $(H_{\parallel}, H_{\perp m}, T)$  phase diagram. It consists of a critical surface, a bicritical point  $B$ , and a first-order shelf (shaded area). (b) The  $(H_{\parallel}, H_{\perp h}, T)$  phase diagram. It consists of two critical surfaces associated with the AF and SF phases, a shelf, and a bicritical line  $BD$ . In the case of  $\text{MnCl}_2 \cdot 4\text{D}_2\text{O}$  the critical surfaces are Ising-like ( $n = 1$ ) and the bicritical line is  $xy$  like ( $n = 2$ ).

temperature with field with the applied field directed along the  $c$ ,  $b$ , and  $a^*$  axes. They investigated the AF-SF transition boundary with the field directed along the  $c$  axis and concluded that the transition was not first order.

Butera and coworkers<sup>21,27-29</sup> have investigated various aspects of the phase diagram with the applied field directed along the  $c$  axis and displaced  $3^\circ$  and  $7^\circ$  toward  $c^*$  in the  $ac$  plane, using measurements of heat capacity,  $(\partial M / \partial T)_H$  and the adiabatic variation of temperature with applied field. The temperature region covered in these studies extended from 0.8 to

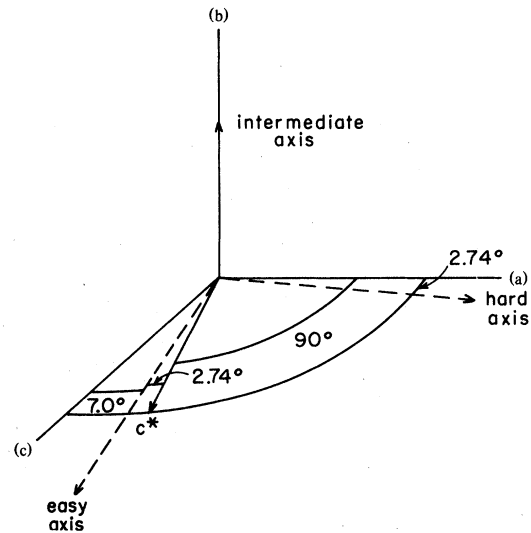


FIG. 2. Relationship of magnetic anisotropy axes to crystallographic axes.

2.0 K. Butera and Rutter<sup>28</sup> investigated the bicritical point region with the applied field directed along the  $c$  axis, and directions displaced  $3^\circ$  and  $7^\circ$  toward  $c^*$  in the  $ac$  plane. They observed a bicritical point only for the field directed along the  $c$  axis, and the variation of the  $\lambda$  lines corresponding to the AF-PM and SF-PM transitions in the region of the bicritical field was in excellent agreement with theory. They reported that for these fields the spins were aligned parallel to the  $c$  axis.

In light of the puzzling results published in the literature, we have undertaken a neutron-diffraction investigation of the range and nature of the AF-SF transition. Other aspects of the phase diagram will be the subject of future studies.  $\text{MnCl}_2 \cdot 4\text{D}_2\text{O}$  was chosen instead of  $\text{MnCl}_2 \cdot 4\text{H}_2\text{O}$  to reduce the background arising from the incoherent scattering.

## II. SYMMETRY ANALYSIS

In this section we analyze the symmetry properties of  $\text{MnCl}_2 \cdot 4\text{D}_2\text{O}$ , construct the Landau-Ginzburg-Wilson (LGW) model appropriate for this compound and discuss the  $(T, \vec{H})$  phase diagram. The paramagnetic space group of  $\text{MnCl}_2 \cdot 4\text{D}_2\text{O}$  is  $G_0 = P2_1/n$ . The unit cell contains four magnetic ions located at (1)  $(x, y, z)$ , (2)  $(\bar{x}, \bar{y}, \bar{z})$ , (3)  $(\frac{1}{2} + x, \frac{1}{2} - y, \frac{1}{2} + z)$ , and (4)  $(-\frac{1}{2} - x, -\frac{1}{2} + y, -\frac{1}{2} - z)$  (for details see Ref. 25). Let  $\vec{S}_i = (S_x, S_y, S_z)$   $i = 1, 2, 3, 4$  be the magnetic moment of the ion located a site  $i$ . Under the operators of the symmetry group  $G_0$ , the vectors  $\vec{S}_i$  transform

in the following way:

$$\begin{aligned}
 i: & \quad \bar{S}_1 \leftrightarrow \bar{S}_2, \quad \bar{S}_3 \leftrightarrow \bar{S}_4, \\
 2_1: & \quad S_{1x} \leftrightarrow -S_{4x}, \quad S_{2x} \leftrightarrow -S_{3x}, \\
 & \quad S_{1y} \leftrightarrow S_{4y}, \quad S_{2y} \leftrightarrow S_{3y}, \\
 & \quad S_{1z} \leftrightarrow -S_{4z}, \quad S_{2z} \leftrightarrow -S_{3z}, \\
 n: & \quad S_{1x} \leftrightarrow -S_{3x}, \quad S_{2x} \leftrightarrow -S_{4x}, \\
 & \quad S_{1y} \leftrightarrow S_{3y}, \quad S_{2y} \leftrightarrow S_{4y}, \\
 & \quad S_{1z} \leftrightarrow -S_{3z}, \quad S_{2z} \leftrightarrow -S_{4z},
 \end{aligned} \tag{1}$$

where  $i$  is the space inversion operator,  $2_1$  is a two-fold screw axis, and  $n$  is a glide plane. The twelve components  $S_{i\mu}$   $i=1, \dots, 4$ ,  $\mu=x,y,z$  form a basis of a reducible representation of the group  $G_0$ . It is easy to see that this representation decomposes into twelve, one-dimensional irreducible representations, whose basis vectors are the  $x,y,z$  components of the following vectors:

$$\begin{aligned}
 \bar{F} &= \bar{S}_1 + \bar{S}_2 + \bar{S}_3 + \bar{S}_4, \\
 \bar{G} &= \bar{S}_1 - \bar{S}_2 + \bar{S}_3 - \bar{S}_4, \\
 \bar{A} &= \bar{S}_1 - \bar{S}_2 - \bar{S}_3 + \bar{S}_4, \\
 \bar{C} &= \bar{S}_1 + \bar{S}_2 - \bar{S}_3 - \bar{S}_4.
 \end{aligned} \tag{2}$$

The magnetic groups associated with these components are given in Table I. Experimentally, it was found that the  $\bar{H}=0$  magnetic structure of  $\text{MnCl}_2 \cdot 4\text{D}_2\text{O}$  is given by the  $\gamma$  component of the vector  $\bar{A}$ , where  $\gamma$  defines the easy magnetic axis in the  $S_x - S_z$  plane. By applying a magnetic field along the easy axis for  $T < T_N$  one finds a spin-flop transition in which the component  $A_y$  orders.

In order to construct the LGW model appropriate for  $\text{MnCl}_2 \cdot 4\text{D}_2\text{O}$  one should examine the coupling terms between the various order parameters of Table I, and in particular the coupling between the magnetic field  $\bar{H}$  and the order parameters  $A_\gamma$  and  $A_y$ . Table I suggests that the three order parameters  $A_x$ ,  $A_z$ , and

TABLE I. The magnetic symmetry groups associated with the 12 order parameters of  $\text{MnCl}_2 \cdot 4\text{D}_2\text{O}$ . Order parameters which transform according to the same irreducible representation of the paramagnetic group, have the same magnetic symmetry and they induce an ordering field on each other.

Symmetry	Order Parameter
$P2'_1/n$	$A_x, A_z, G_y$
$P2_1/n'$	$A_y, G_x, G_z$
$P2_1/n$	$F_y, C_x, C_z$
$P2'_1/n'$	$F_x, F_z, C_y$

$G_y$  transform in the same way under the symmetry operators of the group  $G_0$ . Therefore one expects that  $G_y$  should be induced by  $A_\gamma$  for  $T < T_N$ . However, this order parameter has not been observed experimentally, which suggests that the coupling between  $G_y$  and  $A_\gamma$  may be small. Similarly, in the SF phase, the order parameter  $A_y$  induces  $G_x$  and  $G_z$ . The magnetic field  $\bar{H}$  transforms, under the symmetry operators of  $G_0$ , like the order parameter  $\bar{F}$ . Therefore, according to Table I,  $\bar{H}$  induces a staggered magnetic field which is coupled to the order parameter  $\bar{C}$ , but *does not* induce such a field for  $\bar{A}$  and  $\bar{G}$ . This analysis suggests that the  $(T, \bar{H})$  phase diagram of  $\text{MnCl}_2 \cdot 4\text{D}_2\text{O}$  may be analyzed using two order parameters:

$$\phi_1 = aA_\gamma + bG_y, \tag{3a}$$

and

$$\phi_2 = cA_y + dG_x + eG_z, \tag{3b}$$

where  $a, b, c, d, e$  are parameters which may depend on  $T$  and  $\bar{H}$ . The order parameter  $\phi_1$  is associated with the antiferromagnetic phase while  $\phi_2$  corresponds to the spin-flopped phase. Note that the order parameter  $A_\alpha$ , which is the component of  $\bar{A}$  along the hard magnetic axis  $\alpha$ , is also induced by  $A_\gamma$  in the antiferromagnetic phase but is not observed experimentally. Since this order parameter does not become critical, it may be integrated out, and therefore will not affect the qualitative features of the phase diagram. It will, however, renormalize the various coupling constants which appear in the LGW Hamiltonian  $\mathcal{H}(\phi_1, \phi_2)$ . This Hamiltonian takes the form

$$\begin{aligned}
 \mathcal{H} = & -\frac{1}{2}r_1\phi_1^2 - \frac{1}{2}r_2\phi_2^2 - (a_1H_2H_1 + a_3H_2H_3)\phi_1\phi_2 \\
 & - \frac{1}{2}[(\nabla\phi_1)^2 + (\nabla\phi_2)^2] - u_{11}\phi_1^4 \\
 & - u_{12}\phi_1^2\phi_2^2 - u_{22}\phi_2^4,
 \end{aligned} \tag{4}$$

where the coefficients  $r_1, r_2, a_1, a_3, u_{11}, u_{12}$ , and  $u_{22}$  are functions of  $T$  and  $\bar{H}$ ,  $H_2 = H_y$ , and  $H_1$  and  $H_3$  are the components of the magnetic field along the easy and hard magnetic axes, respectively, in the  $H_x - H_z$  plane. This is the LGW model appropriate for the orthorhombic case, and its  $(\bar{H}, T)$  phase diagram is given schematically in Fig. 1. The AF-PM and SF-PM critical surfaces are associated with  $n=1$  component order parameters,  $\phi_1$  and  $\phi_2$ , respectively, while the bicritical line corresponds to an  $n=2$  component order parameter  $(\phi_1, \phi_2)$ .

The symmetry analysis presented in this section also indicates that  $\text{MnCl}_2 \cdot 4\text{D}_2\text{O}$  should exhibit *magnetoelectric* effects. It is easy to see that by applying an electric field  $\bar{E}$ , the following terms appear in the free energy:

$$H_y E_y A_y, \quad H_y E_{1A_\perp}, \quad H_1 E_y A_{1\perp}, \quad H_{1A_\perp} E_{1A_\perp},$$

where the subscript  $\perp$  denotes the components perpendicular to the  $y$  axis (i.e., the  $\alpha$  and  $\gamma$  components). As a result of these terms one expects, for example, that by applying electric and magnetic fields, one may induce the order parameter  $\bar{A}$  above the critical surfaces.

### III. EXPERIMENTAL

#### A. Sample preparation

The samples used in this study were prepared by reacting spectroscopic-grade manganese metal with high-purity reagent-grade hydrochloric acid to prepare  $\text{MnCl}_2 \cdot 4\text{H}_2\text{O}$  crystals. The  $\text{MnCl}_2 \cdot 4\text{H}_2\text{O}$  was dehydrated at  $300^\circ\text{C}$  under flowing dry  $\text{HCl}$  gas. The anhydrous  $\text{MnCl}_2$  thus prepared was dissolved in  $\text{D}_2\text{O}$  in a glove box to prepare a saturated solution at room temperature. Seed crystals of  $\text{MnCl}_2 \cdot 4\text{D}_2\text{O}$  were prepared from this solution by controlled evaporation under an inert atmosphere. Two large single crystals were grown using this technique. The first was machined into a rectangular platelet  $10 \times 5 \times 2 \text{ mm}^3$ , and the second was machined into a 6-mm-diam sphere. The samples were coated with GE varnish to protect them from loss of  $\text{D}_2\text{O}$  or gain of  $\text{H}_2\text{O}$  and also from H-D exchange.

#### B. Apparatus and experimental method

After a preliminary alignment, the crystal was placed in a He-filled aluminum container in which it was secured by GE varnish and light pressure from a coil spring. This sample holder was mounted in a  $^3\text{He}$  Dewar, positioned approximately vertically in the housing of a horizontal-field electromagnet attached to the sample table of the spectrometer. Sample temperature was controlled to about 1 mK and read with a carbon-glass sensor placed in a hole drilled in the post supporting the crystal. The Dewar was held in the magnet by means of a ring mounted on a spherical bearing surface so that it could be tipped in arbitrary directions through small angles about a point simultaneously centered with respect to the pole faces, the neutron beam, and the sample. The spherical bearing surface could be rotated in the horizontal plane by means of a tangent screw having a sensitivity of approximately  $0.01^\circ$ . The magnet-pole faces were 2 in. in diameter and the gap 3 in. The field was monitored by a Hall probe placed close to a pole face and remained constant to about 1 G. The field at the sample was calibrated against the probe by placing a rotating-coil magnetometer in the sample position. To observe the spin-flop transition, the intensity of a suitable antiferromagnetic Bragg reflection, corrected for nuclear components by subtracting the intensity found above  $T_N$ , was followed as a func-

tion of the strength and direction of the applied field at fixed temperature. The measured intensity depends on the angle between the spin axis and the normal to the scattering planes (scattering vector) and is proportional to  $q^2$ , the square of the sine of that angle. For the  $(\bar{1}02)$  magnetic reflection,  $q^2$  increases by a factor of about 10 when the spin axis changes from the zero-field orientation close to  $c^*$  to the  $b$  axis, in the spin-flop phase.

The spin axis orientation in the basal plane in zero field was obtained from the ratio of the observed intensities of the  $(\bar{1}02)$  and  $(102)$  magnetic reflections. These measurements gave an angle of  $\sim 3^\circ$  from  $c^*$  towards  $c$ , in agreement with the result of Altman *et al.*<sup>25</sup> In measurements to be described later, the tilt of the spin out of the basal plane was found to be  $0^\circ \pm 0.2^\circ$ , which also falls within the error limits given by the above authors.

For measurements with the field in the easy-hard plane ( $ac$  crystallographic plane), the  $b$  axis was set vertical by tilting the cryostat in its supporting ring so as to maximize intensities of a set of  $(h0l)$  reflections. By use of tight vertical collimation, the uncertainty in this orientation could be made less than  $0.05^\circ$ . Precise in-plane alignment of the magnetic field with respect to the crystallographic  $c^*$  axis was obtained in the following way: the horizontal magnet axis was set normal to the neutron beam incident on the sample to establish the zero of its angular scale, using a mechanical guide accurate to about  $0.02^\circ$ . The spectrometer table carrying the magnet was rotated so that this axis pointed in the direction calculated for the scattering vector of the  $(002)$  nuclear reflection, and the counter was positioned to accept that reflection. The Dewar was then rotated relative to the magnet, using the tangent screw, until the  $(002)$  reflection was maximized, and the  $c^*$  axis thus made parallel to the field. Changes in the basal-plane orientation of the field relative to the  $c^*$  axis were made by rotating the magnet-Dewar assembly a known angle from the  $(002)$  reflecting position, using the spectrometer table, and then rotating the Dewar with respect to the magnet in the opposite direction until the reflection was recovered.

To change the angle between the field and medium anisotropy axis (crystallographic  $b$  axis), the magnet-Dewar assembly was first shimmed with respect to the spectrometer table. The Dewar was then separately adjusted to return the  $b$  axis to vertical orientation by the method used in the initial alignment.

### IV. RESULTS

#### A. Qualitative view of the phase diagram

The intensity of the magnetic  $(\bar{1}02)$  reflection was studied at a number of temperatures and magnetic

fields applied along the  $c^*$  axis. Typical results, corrected for nuclear contribution to the scattering, but not for demagnetizing effects, are shown in Fig. 3. From these data, together with a scan at  $H=0$ , we have constructed a qualitative description of the phase diagram over this region of  $H$  and  $T$ , as shown in Fig. 4. The choice of the  $c^*$  direction for the applied field is somewhat arbitrary. It differs from the actual spin axis by  $\sim 3^\circ$ , but it will be shown later that this does not alter the picture appreciably.

### B. Character of the AF-SF transition

A first-order spin-flop transition should exhibit a discontinuous change in Bragg peak intensity at a fixed value of the internal field, corresponding to the change in spin-axis orientation relative to the scattering vector of the magnetic reflection. This change in

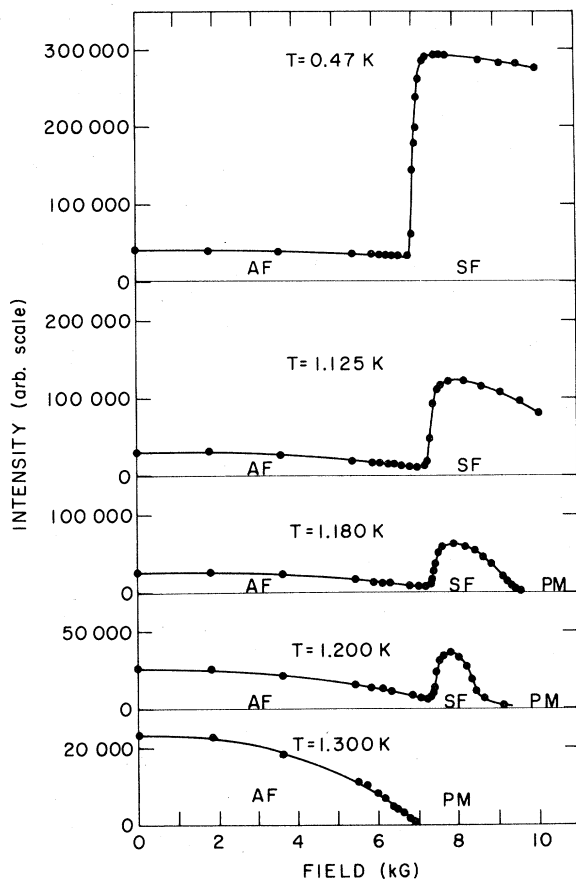


FIG. 3. Intensity of the  $(102)$  magnetic reflection as a function of field applied in the  $c^*$  direction, for representative temperatures. AF, SF, and PM refer to the antiferromagnetic, spin-flop, and paramagnetic regions, respectively. The data, obtained with the platelet sample, have been corrected for nuclear contributions to the scattering, but not for demagnetizing effects.

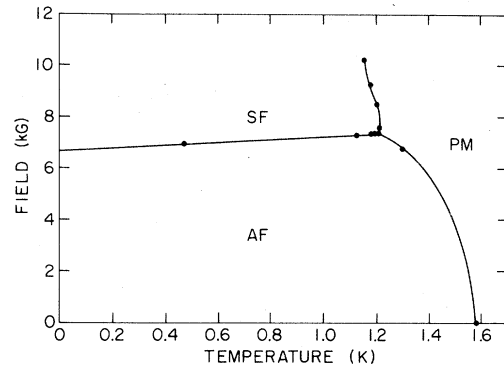


FIG. 4. Approximate phase diagram for field applied along the  $c^*$  axis, constructed from the data of Fig. 3, together with a scan at zero field.

intensity becomes linear in the applied field because of demagnetization effects and reflects the changing proportions of distinct AF and SF phases present in equilibrium.<sup>30</sup> This behavior is clearly demonstrated by the data for the spherical sample in Fig. 5, taken at 0.52 K with field applied along the spin axis, i.e., parallel to a direction  $2.74^\circ$  from  $c^*$  toward  $c$  in the  $ac$  plane. The linear region is seen to extend for approximately 200 G. At higher fields the data exhibit rounding which is most probably caused by extinction. With the uncertainty that this introduces, the

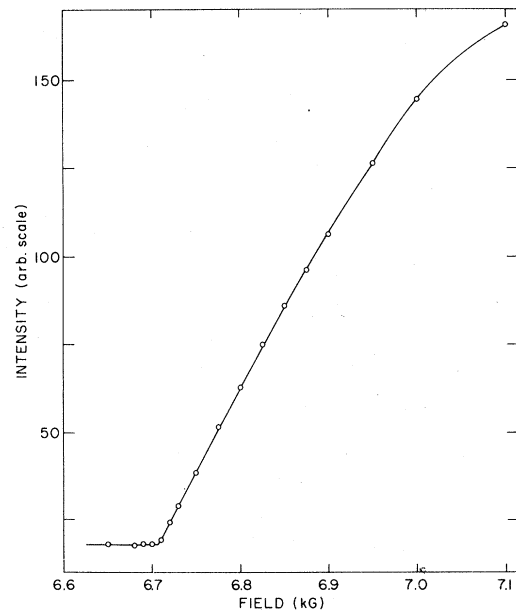


FIG. 5. Spin-flop transition at  $T=0.52$  K. Data are for the spherical sample with field applied along the easy anisotropy axis (displaced  $2.74^\circ$  from  $c^*$  toward  $c$  in the basal plane).

two-phase region may be estimated to exist over a range of fields equal to 250–300 G. This range is comparable with the change in demagnetizing field predicted by molecular field (MF) calculations.<sup>31</sup> Taking  $\chi_{AF}$  and  $\chi_{SF}$ , the molar susceptibility values, reported for the hydrated material<sup>20</sup> and applying the demagnetizing factor for a sphere, we have

$$\begin{aligned} \Delta H(T) &= \frac{4}{3} \pi \frac{1}{v_m} [\chi(T)_{SF} H_2 - \chi(T)_{AF} H_1] \\ &= (0.0438)(1.438 \times 7020 - 0.796 \times 6710) \\ &= 208 \text{ G} , \end{aligned} \quad (5)$$

where  $v_m$  is the molar volume and  $H_1$  and  $H_2$  are estimates of the end points of the transition region.

Data for 0.80 and 1.10 K are shown in Figs. 6 and 10. As in the case of the 0.52-K data, the range of the two-phase region is qualitatively in accord with published magnetization data for the hydrated material.<sup>20,26</sup> The data taken at 1.10 K, which is approximately 0.1 K below the bicritical point, have been corrected for critical scattering on the basis of an analysis to be presented in a later section. It will also be shown that this analysis provides independent confirmation of the first-order nature of the transition close to the bicritical point.

This same MF treatment can also be applied to the adiabatic magnetization data reported by Giauque *et al.*<sup>20</sup> for the hydrated material, with the field applied parallel to the  $c$  axis and perpendicular to the  $b$  axis. These data exhibit linearity at  $T=0.40$  K over a field range of 200 G. Applying the MF approxima-

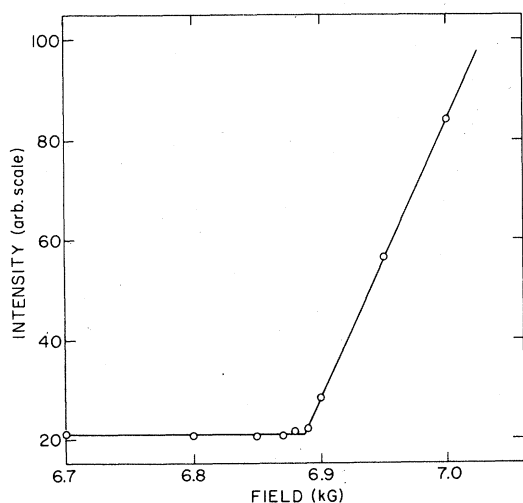


FIG. 6. Spin-flop transition at  $T=0.80$  K. Data are for the spherical sample with field applied in the easy direction.

tion to these data yields

$$\begin{aligned} \Delta H(T) &= (0.0438)(1.438 \times 7400 - 0.796 \times 7100) \\ &= 215 \text{ G} , \end{aligned} \quad (6)$$

which is in excellent agreement. We conclude therefore that the hydrate, as well, exhibits a first-order transition at the AF-SF boundary at very low temperatures.

### C. Dependence of the AF-SF transition field on orientation in the $ac$ plane

The intensity as a function of applied field at  $\sim 0.5$  K has been determined over the AF-SF transition region for several orientations in the  $ac$  plane using the platelet sample. The dependence of the onset of the linear region  $H_1$ , on orientation in the  $ac$  plane is shown in Fig. 7, where the angle  $\omega$  is measured from

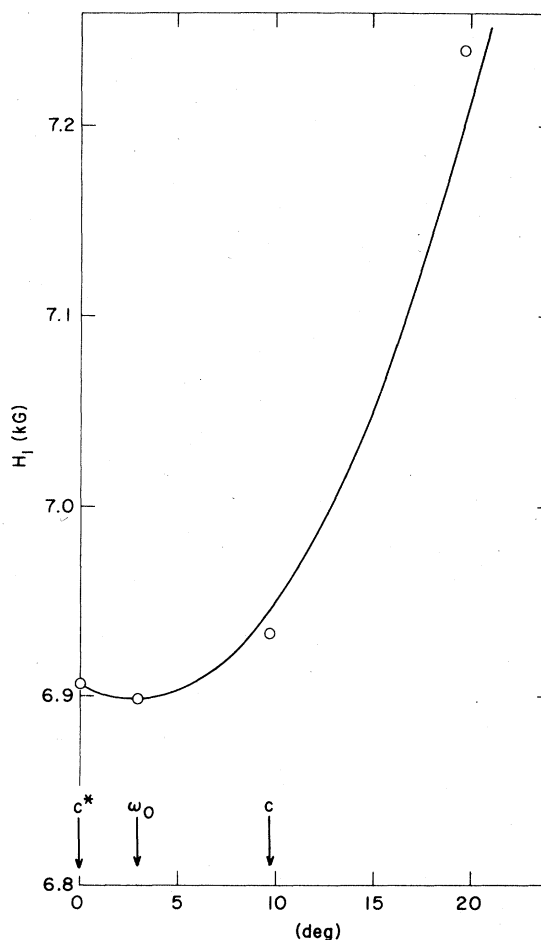


FIG. 7. Onset of the linear region of the spin-flop transition ( $H_1$ ) at  $T \sim 0.5$  K, as a function of the angle ( $\omega$ ) between the field and a reference direction, taken as the  $c^*$  axis. The curve represents the expression  $H_1 = 6898 / \cos(\omega - \omega_0)$ , where  $\omega_0$  corresponds to the easy direction.

the  $c^*$  axis, towards  $c$ , and  $\omega_0$  represents the direction of the easy axis in the plane. The smooth curve is calculated from

$$H_1 = 6898 / \cos(\omega - \omega_0) \quad (7)$$

indicating that the shelf is flat in the region studied. The fit is quite adequate and indicates that the SF shelf extends at least 2500 G in the  $H_{1h}$  direction, as expected for a monoclinic antiferromagnet and shown schematically in Fig. 1. It was not possible to reach the edge of the shelf because of physical limitations of the apparatus, but later measurements at 0.8 K, using a different sample, showed that the shelf extended to at least 4500 G.

#### D. Width of the AF-SF shelf in the $H_{\parallel} - H_{\perp m}$ plane at $T = 1.100$ K

Previous experimental studies<sup>17-21, 24-29</sup> have failed to yield evidence of a first-order transition at the AF-SF boundary for temperatures greater than 0.4 K. This may have been due to a lack of precise alignment of the applied field perpendicular to the medium anisotropy axis ( $b$  axis). As we have seen, this orientation is expected to be far more critical than alignment in the  $ac$  plane. To obtain an estimate of the allowable degree of misorientation, we measured the intensity of the  $(\bar{1}02)$  reflection as a function of applied field at  $T = 1.100$  K, using the spherical sample, for tilt angles relative to the  $ac$  plane of  $-0.93^\circ$ ,  $-0.40^\circ$ ,  $0.00^\circ$ ,  $0.06^\circ$ ,  $0.22^\circ$ ,  $0.52^\circ$ ,  $0.81^\circ$ , and  $1.52^\circ$ . These data are shown in Fig. 8.

For the larger angles, the behavior was clearly gradual and it was possible to fit the data on the assumption that the staggered magnetization rotated continuously from the  $ac$  plane towards the  $b$  axis as a function of increasing field. Referring to Fig. 9(a), in which  $\bar{M}_{ST}$  is the staggered magnetization and  $\bar{\epsilon}_{\bar{1}02}$  is the scattering vector of the magnetic reflection, the intensity is given by  $I \sim M_{ST}^2 \sin^2 \phi = M_{ST}^2 (1 - \epsilon_{\bar{1}02}^2 M_{ST}^2 / M_{ST}^2)$ , inasmuch as  $\bar{M}_{ST}$  has components only in the easy-medium plane and  $\bar{\epsilon}_{\bar{1}02}$  lies in the easy-hard plane. In terms of the angles  $\zeta$  and  $\theta$ , this can be written

$$I = A \sin^2 \zeta + B \quad (8)$$

with  $A = M_{ST}^2 \cos^2 \theta$  and  $B = M_{ST}^2 \sin^2 \theta$ . The angle  $\zeta$  can be expressed, approximately, in terms of applied field, using the mean-field expression<sup>32</sup> derived for low temperatures and for tilt angles in the easy-medium plane which are large compared to that corresponding to the edge of the first-order shelf:

$$\tan(2\zeta + 2\psi) = \frac{\sin 2\psi}{\cos 2\psi - (H/H_{SF})^2}, \quad (9)$$

where  $\psi$ , the angle between the field and the easy

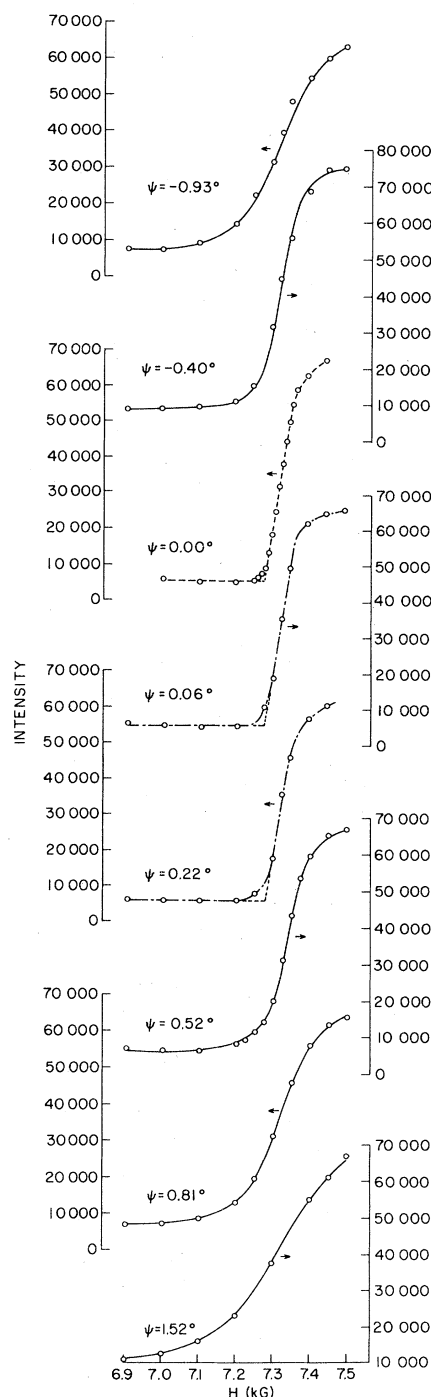


FIG. 8. Field dependence of the AF-SF transition at 1.100 K for various angles of tilt ( $\psi$ ) of the field with respect to the easy axis, in the easy-medium plane. Intensities refer to the  $(\bar{1}02)$  reflection in the spherical sample. Solid lines are fits to the low-temperature, mean-field expression given in Eq. (9). The data for  $|\psi| < 0.40^\circ$ , connected by dashed lines, cannot be fitted in this way because of the pronounced linear behavior, and provide a conservative upper limit to the width of the first-order shelf.

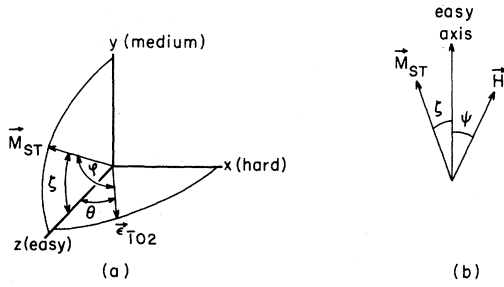


FIG. 9. Definitions of angles connecting the staggered magnetization ( $\vec{M}_{ST}$ ), the scattering vector for the (102) reflection ( $\vec{\epsilon}_{T02}$ ), and applied field ( $\vec{H}$ ) with the anisotropy axes.

axis is shown in Fig. 9(b). The solid lines drawn through the data of Fig. 8 for  $|\psi| \geq 0.40$  indicate that satisfactory fits can be obtained in this manner. This is not the case for  $|\psi| < 0.40$ , however, inasmuch as the data exhibit pronounced linear regions which cannot be well represented. Considering the domain of applicability of the mean-field expression, we conclude that the first-order shelf has a half-width which may well be appreciably less than  $0.40^\circ$ .

This behavior is consistent with the characteristics of the first-order transition predicted by the MF treatment of Rohrer and coworkers<sup>3-9</sup> for the region where  $|\psi| < \psi_c$ . One can estimate the width of the spin-flop shelf using the anisotropy data reported for the hydrated material<sup>26</sup> and the MF expression given by Rohrer and Thomas.<sup>3</sup> The value of the critical angle at  $T=0$  K has been estimated<sup>26</sup> to be  $\psi_c(T=0) = 6.5^\circ$ . An upper limit to the value of  $\psi_c(T)$  at  $T = 1.100$  K can be estimated using the expression

$$\psi_c(T) \approx \psi_c(0)(T_b - T)/T_b \quad (10)$$

given by Blazey *et al.*<sup>4</sup> together with the value of the bicritical temperature ( $T_b = 1.21$  K) for the hydrate reported by Butera and Rutter.<sup>23</sup> This calculation gives  $\psi_c(T = 1.100 \text{ K}) \leq 0.60^\circ$  which compares favorably with the result of this study.

### E. Critical scattering and the first-order phase transition

In the vicinity of the bicritical point, the spin-flop transition is accompanied by appreciable critical scattering. This scattering increases with field as the transition is approached from below, reaching a maximum at the onset of the transition, and then decreases with the increase of the percentage of spin-flop phase present in the two-phase region. In this section we treat this critical scattering theoretically and present an approximate procedure for separating the critical and Bragg components of the experimental data. Finally, we show that the behavior of the

range and amplitude parameters characterizing the critical scattering provide independent confirmation of the first-order nature of the spin-flop transition at 1.10 K.

The intensity of the critical scattering is given by the expression

$$I \sim \left\{ \delta_{\alpha\beta} - \frac{K_\alpha K_\beta}{K^2} \right\} \chi_{\alpha\beta}(\vec{q}) F_{\alpha\beta}(\vec{q}, \omega), \quad (11)$$

where  $\vec{K}$  is the scattering vector,  $\chi_{\alpha\beta}(\vec{q})$  the static susceptibility corresponding to a momentum change  $\hbar\vec{q}$  referred to the magnetic reciprocal-lattice point as origin,  $F(\vec{q}, \omega)$  a shape factor for the energy ( $\hbar\omega$ ) dependence of the scattering and  $\alpha, \beta$  denote components relative to an orthogonal set of axes, which we take to be the anisotropy axes of Fig. 9(a).

Making the usual assumption that the  $z$  component of the spin is a constant of the motion, so that cross terms in  $\chi_{\alpha\beta}$  vanish, we have, in quasielastic approximation

$$I \sim \left\{ 1 - \frac{K_x^2}{K^2} \right\} \chi_{xx}(q) + \left\{ 1 - \frac{K_y^2}{K^2} \right\} \chi_{yy}(q) + \left\{ 1 - \frac{K_z^2}{K^2} \right\} \chi_{zz}(q), \quad (12)$$

where  $x, y,$  and  $z$  refer to the hard, medium, and easy axes. Noting that the scattering vector used in the experiments ( $\vec{1}02$ ) is very nearly parallel to the  $z$  axis, we obtain

$$I \sim \chi_{xx}(q) + \chi_{yy}(q). \quad (13)$$

As the bicritical point is approached, the susceptibilities along the easy [ $\chi_{zz}(0)$ ] and medium [ $\chi_{yy}(0)$ ] axes diverge, while  $\chi_{xx}(0)$ , the susceptibility along the hard  $a$  axis, remains finite. One may therefore neglect  $\chi_{xx}(q)$  in Eq. (13) and obtain

$$\begin{aligned} \text{AF phase: } I &\sim \chi_{yy}^{\text{AF}}(q) = \chi_{\perp}^{\text{AF}}(q), \\ \text{SF phase: } I &\sim \chi_{yy}^{\text{SF}}(q) = \chi_{\parallel}^{\text{SF}}(q). \end{aligned} \quad (14)$$

In the following section we show that on the coexistence line one has  $\chi_{\parallel}^{\text{SF}}/\chi_{\perp}^{\text{AF}} \ll 1$ , and therefore the contribution of the SF phase to the critical scattering intensity is much smaller than that of the AF phase.

We consider a simple microscopic model for uniaxial antiferromagnets, and study it within the mean-field approximation. Let  $\vec{S}_i$  be a spin- $\frac{1}{2}$  vector located on the site  $i$  of, say, a tetragonal lattice. Consider the following Hamiltonian:

$$\mathcal{H} = -J \sum_{\langle ij \rangle} \vec{S}_i \cdot \vec{S}_j - K \sum_i S_{iz}^2 - H \sum_i S_{iz}, \quad (15)$$

where the sum  $\sum_{\langle ij \rangle}$  is over nearest-neighbor sites  $\langle ij \rangle$ , the coupling  $J$  is antiferromagnetic,  $J < 0$ , and

the anisotropic term favors an ordering along the  $z$  axis,  $K > 0$ . This is the simplest model which exhibits a bicritical point in the  $TH$  plane. Let  $\bar{M}_1$  and  $\bar{M}_2$  be the magnetic moments associated with the sublattices 1 and 2, respectively. Within the mean-field theory, the free energy  $\phi$  associated with this model is given by

$$\begin{aligned} \beta\phi/N = & -\beta J \bar{z} \bar{M}_1 \cdot \bar{M}_2 - \beta K (M_{1z}^2 + M_{2z}^2) \\ & - \beta H (M_{1z} + M_{2z}) \\ & + \frac{1}{2} \sum_{i=1}^2 [(1 + M_i) \ln(1 + M_i) \\ & + (1 - M_i) \ln(1 - M_i)] \quad , \quad (16) \end{aligned}$$

where  $\beta = 1/k_B T$ ,  $N$  is the number of sites in each sublattice,  $\bar{z}$  is the coordination number, and

$$M_i^2 = M_{iy}^2 + M_{iz}^2, \quad i = 1, 2 \quad . \quad (17)$$

Here we assume that in the SF phase the sublattice magnetization lies in the  $y$ - $z$  plane, namely,  $M_{ix} = 0$ . Let

$$\bar{F} = \bar{M}_1 + \bar{M}_2, \quad \bar{A} = \bar{M}_1 - \bar{M}_2 \quad . \quad (18)$$

To fourth order in  $\bar{F}$  and  $\bar{A}$ , the free energy takes the form:

$$\begin{aligned} \beta\phi/N = & -\beta H F_z + (1 - \frac{1}{4} \beta J \bar{z} - \frac{1}{2} \beta K) F_z^2 \\ & + (1 + \frac{1}{4} \beta J \bar{z} - \frac{1}{2} \beta K) A_z^2 + (1 + \frac{1}{4} \beta J \bar{z}) A_y^2 \\ & + \frac{1}{6} (F_z^4 + A_y^4 + A_z^4 + 6 F_z^2 A_z^2 \\ & + 2 F_z^2 A_y^2 + 2 A_y^2 A_z^2) \quad . \quad (19) \end{aligned}$$

Minimizing  $\phi$  with respect to  $F_z$  we find

$$F_z = \frac{3\beta H}{6(1 - \frac{1}{4} \beta J \bar{z} - \frac{1}{2} \beta K) + (6A_z^2 + 2A_y^2)} \quad . \quad (20)$$

Inserting Eq. (20) into Eq. (19) we finally obtain the following expression for the free energy:

$$\begin{aligned} \beta\phi/N = & \phi_0 + \frac{1}{2} r_1 A_z^2 + \frac{1}{2} r_2 A_y^2 + u_{11} A_z^4 \\ & + u_{12} A_y^2 A_z^2 + u_{22} A_y^4 + 0(A_y^6, A_z^6) \quad , \quad (21) \end{aligned}$$

where

$$\begin{aligned} r_1 = & 2 \left[ 1 + \frac{1}{4} \beta J \bar{z} - \frac{1}{2} \beta K + \frac{(\beta H)^2}{4(1 - \frac{1}{4} \beta J \bar{z} - \frac{1}{2} \beta K)^2} \right] \quad , \\ r_2 = & 2 \left[ 1 + \frac{1}{4} \beta J \bar{z} + \frac{1}{3} \frac{(\beta H)^2}{4(1 - \frac{1}{4} \beta J \bar{z} - \frac{1}{2} \beta K)^2} \right] \quad , \\ u_{11} = & \frac{1}{6} - \frac{(\beta H)^2}{4(1 - \frac{1}{4} \beta J \bar{z} - \frac{1}{2} \beta K)^3} \quad , \quad (21a) \\ u_{22} = & \frac{1}{6} - \frac{(\beta H)^2}{36(1 - \frac{1}{4} \beta J \bar{z} - \frac{1}{2} \beta K)^3} \quad , \\ u_{12} = & \frac{1}{3} - \frac{(\beta H)^2}{6(1 - \frac{1}{4} \beta J \bar{z} - \frac{1}{2} \beta K)^3} \quad . \end{aligned}$$

The bicritical point is located at

$$r_1 = r_2 = 0$$

and the AF-SF coexistence line is given by

$$\frac{r_1^2}{u_{11}} = \frac{r_2^2}{u_{22}}, \quad r_1, r_2 < 0 \quad . \quad (22)$$

Along this line we find

$$(\chi_{\parallel}^{\text{SF}})^{-1} = \left( \frac{\partial^2 \phi}{\partial A_y^2} \right)_{A_z=0} = 2|r_1| \left( \frac{u_{22}}{u_{11}} \right)^{1/2} \quad , \quad (23)$$

and

$$(\chi_{\perp}^{\text{AF}})^{-1} = \left( \frac{\partial^2 \phi}{\partial A_y^2} \right)_{A_y=0} = |r_1| \frac{1}{2u_{11}} (u_{12} - 2\sqrt{u_{11}u_{22}}) \quad . \quad (24)$$

Inserting Eq. (23) into Eq. (24) we finally obtain

$$\frac{\chi_{\parallel}^{\text{SF}}}{\chi_{\perp}^{\text{AF}}} = \left| \frac{K}{J\bar{z}} \right| + O \left( \left[ \frac{K}{J\bar{z}} \right]^2 \right) \quad . \quad (25)$$

By studying the Hamiltonian (15) at  $T=0$  one finds that the critical field  $H_{\text{SF}}$  for the AF-SF transition and the critical field  $H_F$  for the SF-PARA transition are related by

$$\left( \frac{H_{\text{SF}}}{H_F} \right)^2 = \left| \frac{K}{J\bar{z}} \right| + O \left( \left[ \frac{K}{J\bar{z}} \right]^2 \right) \quad . \quad (26)$$

For  $\text{MnCl}_2 \cdot 4\text{D}_2\text{O}$  one has<sup>26</sup>

$$\frac{H_{\text{SF}}}{H_F} \approx 0.3 \quad (27)$$

and hence

$$\frac{\chi_{\parallel}^{\text{SF}}}{\chi_{\perp}^{\text{AF}}} \approx 0.09 \quad . \quad (28)$$

Therefore the contribution of the SF phase to the scattering intensity on the coexistence line is much

smaller than that of the AF phase. Note that the fact that  $\chi_1^{\text{AF}}$  is inversely proportional to the small parameter ( $K/Jz$ ) may provide an explanation for the large critical scattering observed on the coexistence line below the bicritical point.

#### F. Treatment of experimental data

The observed magnetic scattering in the ordered region close to the bicritical point consists of a sharp Bragg peak superimposed on a broad, Lorentzian-like base produced by critical scattering. The latter component is given by a convolution of the cross section,  $\chi(\vec{q})$ , with the instrumental resolution function. With a given functional form for the cross section, the correlation length, which appears as a parameter, can be obtained from a least-squares fit of the convoluted cross section to the wing portions of the reflection. Using the final form of the cross section, the convolution can also be computed in the region under the Bragg peak to obtain corrected values for the Bragg intensities.

From mean-field theory,  $\chi(\vec{q})$  can be expressed in the form

$$\chi(q) = \frac{A}{\kappa^2 + g(q)} \quad (29)$$

in which  $\kappa$  is the inverse correlation range parameter and  $g(\vec{q})$  is the Fourier transform of the exchange interaction. The transform can be evaluated approximately by treating the unit cell as orthorhombic and the manganese atoms as face centered. (Choosing the origin at  $x=0.25$ ,  $y=0.17$ ,  $z=0$  in space group

$P2_1/n$ , the manganese atoms are located at  $0,0,0$ ;  $0, \frac{1}{2}, \frac{1}{2}; \frac{1}{2}, 0.16, \frac{1}{2}$ , and  $\frac{1}{2}, \frac{1}{2} + 0.16, 0$ ). With these simplifying assumptions, we have

$$g(q) = -J_1 q_a^2 a^2 + J_2 (q_a^2 a^2 + q_b^2 b^2 + q_c^2 c^2) \quad (30)$$

where  $J_1$  and  $J_2$  are first- and second-neighbor exchange constants. The spin assignments for atoms in positions listed above are  $+, +, -, -$ ; respectively, as in ordering of the first kind for fcc crystals. This similarity suggests<sup>33</sup> that  $J_1$  is negative and  $J_2$  positive. The value of the ratio  $(|J_1| + J_2)/J_2$  was fixed at 18 by least-squares fitting, although the results were rather insensitive to the exact choice.

Data for the 1.100 K Bragg peak, corrected for critical scattering is shown in Fig. 10. The closed circles represent the correction, applied to the raw data, and indicates the general behavior of the critical scattering with field.

It is interesting to look more closely at the field dependence of the critical scattering, and, in particular, at the expected behavior of the inverse range parameter  $\kappa$  and the normalization constant  $A$ . As the transition is approached from below and the system is wholly within the AF phase, the normalization

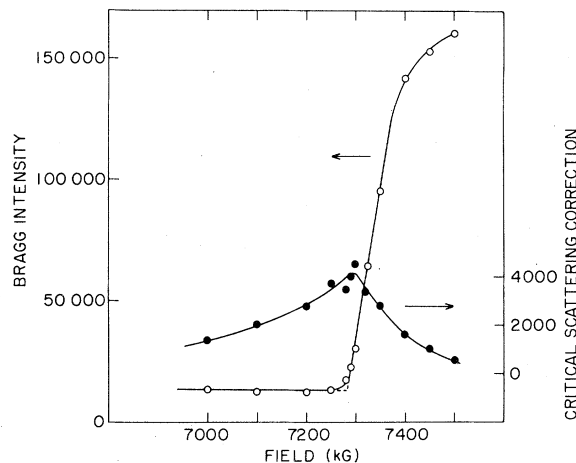


FIG. 10. Spin-flop transition at 1.100 K. The open circles (left-hand scale) give intensities for the  $(\bar{1}02)$  magnetic peak, in the spherical sample, corrected for critical scattering as explained in the text. The actual corrections to the Bragg reflection are given by the closed circles (right-hand scale) and demonstrate the peaking of the critical scattering at the onset of the spin-flop transition.

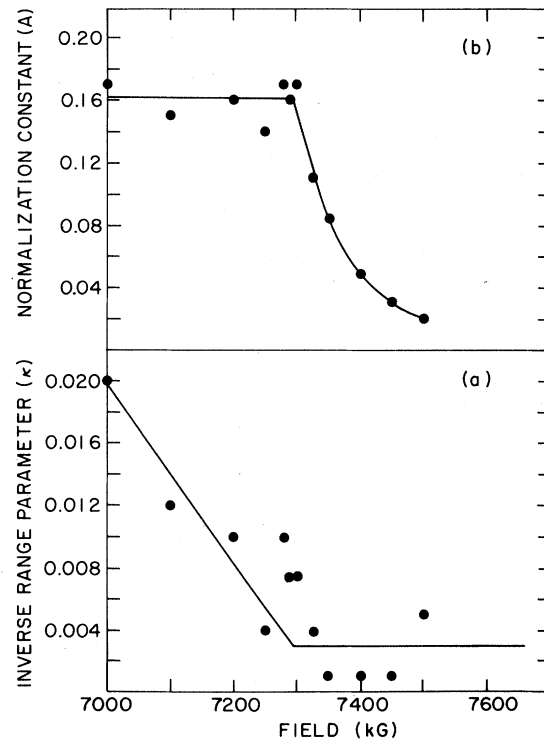


FIG. 11. Results of the analysis of the critical scattering associated with the spin-flop transition at 1.100 K: (a) inverse range parameter, (b) normalization constant. The lines in the figure are intended as visual aids.

constant should remain constant and the inverse range parameter should tend toward zero. In the two-phase region, since the internal field is unchanged,  $\kappa$  should remain constant. The normalization, on the other hand, should decrease because the scattering from the SF phase is much weaker than that from the AF phase. While we do not claim quantitative accuracy for the least-squares results, they do exhibit the expected behavior as shown in Fig. 11. In contrast to this behavior, a model in which the spins turn continuously with field, would

be expected to show a minimum in  $\kappa$  and a continuously falling normalization constant.

#### ACKNOWLEDGMENTS

Research carried out at Brookhaven National Laboratory under contract with the U.S. Department of Energy and supported by its Office of Basic Energy Sciences and supported in part by a grant from the U.S.-Israel Binational Science Foundation (BSF), Jerusalem, Israel.

- 
- <sup>1</sup>See the excellent review article by L. J. deJongh and A. R. Miedema, *Adv. Phys.* **23**, 1-260 (1974).
- <sup>2</sup>M. E. Fisher and D. R. Nelson, *Phys. Rev. Lett.* **32**, 1350 (1974); J. M. Kosterlitz, D. R. Nelson, and M. E. Fisher, *Phys. Rev. B* **13**, 412 (1976), and references therein.
- <sup>3</sup>H. Rohrer and H. Thomas, *J. Appl. Phys.* **40**, 1025 (1969); C. J. Gorter and J. Haantjes, *Physica* **18**, 285 (1952).
- <sup>4</sup>K. W. Blazey, H. Rohrer, and R. Webster, *Phys. Rev. B* **4**, 2287 (1971).
- <sup>5</sup>H. Rohrer, in *Magnetism and Magnetic Materials—1974*, edited by C. D. Graham, G. H. Lander, and J. J. Rhyne, AIP Conf. Proc. No. 24 (AIP, New York, 1975), p. 268.
- <sup>6</sup>H. Rohrer, *Phys. Rev. Lett.* **34**, 1638 (1975).
- <sup>7</sup>H. Rohrer, B. Derighetti, and Ch. Gerber, *Physica* **86-88B**, 597 (1977).
- <sup>8</sup>H. Rohrer and Ch. Gerber, *Phys. Rev. Lett.* **38**, 909 (1977).
- <sup>9</sup>H. Rohrer and Ch. Gerber, *J. Appl. Phys.* **49**, 1341 (1978).
- <sup>10</sup>H. M. Gijsman, N. J. Poulis, and J. Van den Handel, *Physica* **25**, 954 (1959).
- <sup>11</sup>I. Tsujikawa and E. Kanda, *J. Phys. Radium* **20**, 352 (1959).
- <sup>12</sup>M. Abkowitz and A. Honig, *Phys. Rev.* **136**, A1003 (1964).
- <sup>13</sup>S. A. Friedberg and J. H. Schelleng, in *Proceedings of the International Conference on Magnetism, Nottingham, 1964* (IOP, London, 1965).
- <sup>14</sup>A. Zalkin, J. D. Forrester, and D. H. Tempelton, *Inorg. Chem.* **3**, 529 (1964).
- <sup>15</sup>R. D. Spence and V. Nagarajan, *Phys. Rev.* **149**, 191 (1966).
- <sup>16</sup>J. E. Rives, *Phys. Rev.* **162**, 491 (1967).
- <sup>17</sup>T. A. Reichert and W. F. Giauque, *J. Chem. Phys.* **50**, 4205 (1969).
- <sup>18</sup>W. F. Giauque, R. A. Fisher, E. W. Hornung, and R. A. Fisher, *J. Chem. Phys.* **52**, 2901 (1970).
- <sup>19</sup>W. F. Giauque, E. W. Hornung, G. E. Brodale, and R. A. Fisher, *J. Chem. Phys.* **52**, 3936 (1970).
- <sup>20</sup>W. F. Giauque, R. A. Fisher, E. W. Hornung, and G. E. Brodale, *J. Chem. Phys.* **53**, 1474 (1970).
- <sup>21</sup>T. A. Reichert, R. A. Butera, and E. J. Schiller, *Phys. Rev. B* **1**, 4446 (1970).
- <sup>22</sup>M. J. Metcalfe, *Phys. Lett.* **36A**, 373 (1971).
- <sup>23</sup>Z. M. El Saffar and G. M. Brown, *Acta Crystallogr. Sect. B* **27**, 66 (1971).
- <sup>24</sup>J. E. Rives, S. H. Bhatia, and V. Benedict, in *Magnetism and Magnetic Materials—1973*, edited by C. D. Graham and J. J. Rhyne, AIP Conf. Proc. No. 18 (AIP, New York, 1974), p. 335.
- <sup>25</sup>R. F. Altman, S. Spooner, D. P. Landau, and J. E. Rives, *Phys. Rev. B* **11**, 458 (1975).
- <sup>26</sup>J. E. Rives and V. Benedict, *Phys. Rev. B* **12**, 1908 (1975).
- <sup>27</sup>R. A. Butera, T. A. Reichert, and E. J. Schiller, in *Magnetism and Magnetic Materials—1975*, edited by J. J. Becker, G. H. Lander, and J. J. Rhyne, AIP Conf. Proc. No. 29 (AIP, New York, 1976), p. 447.
- <sup>28</sup>R. A. Butera and D. R. Rutter, *J. Appl. Phys.* **49**, 1344 (1978).
- <sup>29</sup>R. A. Butera, R. J. Moskaitis, D. R. Rutter, and R. T. Obermyer, *J. Appl. Phys.* **50**, 1847 (1979).
- <sup>30</sup>A. L. M. Bongaarts and W. J. M. de Jonge, *Phys. Rev. B* **15**, 3434 (1977); A. F. G. Wyatt, *J. Phys. C* **1**, 684 (1968).
- <sup>31</sup>A. R. King and D. Paquette, *Phys. Rev. Lett.* **30**, 662 (1973).
- <sup>32</sup>T. Nagamiya, K. Yosida, and R. Kubo, *Adv. Phys.* **4**, 1 (1955).
- <sup>33</sup>J. S. Smart, in *Magnetism*, edited by G. T. Rado and H. Suhl (Academic, New York, 1963), Vol. III.